Nanoscale

PAPER

View Article Online
View Journal

Cite this: DOI: 10.1039/c5nr07628e

Metal–semiconductor–metal transition in zigzag carbon nanoscrolls†

Haixia Dong,[a,b] Yang Zhang,*[a] Dangqi Fang,[a] Baihua Gong,[a] Erhu Zhang[a] and Shengli Zhang*[a]

Received 31st October 2015,
Accepted 29th December 2015

DOI: 10.1039/c5nr07628e

www.rsc.org/nanoscale

Similar to rolling up paper, carbon nanoscrolls (CNSs) can be rolled from graphene nanoribbons (GNRs) using physical approaches. Owing to their peculiar one-dimensional nanostructures, CNSs have attracted great attention over the past few years. In this study, we have investigated the effects of bending deformation on the electronic properties of zigzag CNSs (ZCNSs) during the rolling process from zigzag GNRs (ZGNRs) by means of first-principles calculations. It is found that a metal–semiconductor–metal transition is observed. By analyzing charge density and density of states, the origin of this electronic property transition is discussed. Furthermore, we find that the metal–semiconductor–metal transition in ZCNSs is independent of ribbon width as well as spin–orbit interaction. Our results of the metal–semiconductor–metal transition in the ZCNSs are robust and may open potential applications in nano-electromechanical devices based on the ZCNSs.

Introduction

Graphene nanoribbons (GNRs), one-dimensional nanostructures, can be obtained by cutting graphene sheets. Carbon nanoscrolls (CNSs), a new form of the carbon-based nanomaterials and first proposed by Bacon in 1960,[1] can be regarded as GNRs rolling up in a spiral form. Owing to the remarkable structural, mechanical, and electronic properties and potential applications in nanodevices, both GNRs and CNSs have attracted extensive attention over the past few years.[2–11]

Recently, theoretical studies have verified that armchair graphene nanoribbons (AGNRs) exhibit metallic or semiconducting properties mainly depending on the ribbon width, while zigzag graphene nanoribbons (ZGNRs) are metallic independent of it.[12–15] Similar electronic properties greatly related to chirality (n,m) have also been observed in single-walled carbon nanotubes.[16] Different from GNRs and carbon nanotubes, CNSs are non-planar systems and topologically open-ended with two edges. Generally, CNSs can be constructed from GNRs by applying a bending strain perpendicular to the ribbon axis. Owing to the interactions of inter-layers, CNSs can be actively controlled and maintained at room temperature.[4,5,17–19] Otherwise, they will collapse immediately due to the curvature energy.

By employing first-principles calculations, zigzag CNSs (ZCNSs) have been revealed to have good conductivity due to the great values of density of states at the Fermi level, while armchair CNSs (ACNSs) exhibit smaller energy gaps than those of the corresponding single-walled carbon nanotubes.[20–22] Because of open and highly tunable geometrical structures, CNSs are applicable to deliver water molecules, deoxyribonucleic acids, fullerenes, and nanoparticles.[4] Besides, closely packed CNSs have been shown to be potential energy-absorbing materials as well as artificial muscles, which greatly relies on their reversible and controllable volumetric deformations.[5] Experimentally, CNSs are detected to be multilayered and maintain a high current density, which facilitates their application as microcircuit interconnects.[23,24] To date, the available research studies have been devoted to the formation, structural stability, mechanical and electronic properties of multilayered CNSs[5,17,20–22,25–33] However, for few-layered or even single-layered CNSs, the structures and electronic properties should be distinct from multilayered CNSs. Specifically, during the formation process of single-layer CNSs rolled from GNRs, their electronic properties would vary dramatically. Since the single-layer CNSs can be regarded as the embryonic forms of multilayered CNSs, investigations on these CNSs, especially on their formation process, are meaningful to understand the multilayered CNSs and exploit their potential applications. To the best of our knowledge, however, few efforts have been devoted to the formation process of CNSs.

[a]Department of Applied Physics, Xi'an Jiaotong University, Xi'an 710049, China. E-mail: zhangsl@mail.xjtu.edu.cn, yzhang520@mail.xjtu.edu.cn; Fax: +86 29 82668559; Tel: +86 29 82668559
[b]Institute of Solid State Physics, Shanxi Datong University, Datong 037009, China
†Electronic supplementary information (ESI) available. See DOI: 10.1039/c5nr07628e

In this work, first-principles calculations have been employed to investigate the electronic properties of both ZCNSs and ACNSs during their rolling processes from GNRs by bending deformation. It is found that a metal–semiconductor–metal transition can be observed in the ZCNSs, but a similar electronic property transition is not presented in the ACNSs (see Table S1†). Thereby, the focus of this study is solely on the ZCNSs. The article is constructed as follows. A brief description of the computational methods and models is given in the following section. The third section presents the calculated results, discussion and comparison with available results. The main conclusions are summarized in the fourth section.

Computational methods and models

Our studies were performed by using first-principles calculations based on density functional theory (DFT) within the projector augmented wave method, as implemented in the Vienna *ab initio* simulation package (VASP).[34–36] The exchange–correlation interactions were described by the local density approximation (LDA).[37] The cut-off of plane-wave energy and the convergence of total energy were set to be 400 eV and 10^{-5} eV, respectively. Structural relaxations were performed by computing the Hellmann–Feynman forces using a conjugate gradient algorithm within a force convergence of 0.02 eV $Å^{-1}$. Because of the periodic boundary conditions, all CNSs were modeled in a large rectangular supercell with their axial directions along the *z*-axis. To eliminate the interactions among the neighbor CNSs, a vacuum region of at least 10 Å was applied perpendicular to the *z*-axis, which had been tested to be valid. Brillouin zone integrations were approximated by using 1 × 1 × 11 *k*-point meshes with Monkhorst–Pack for structure optimizations.[38] For calculations of band structures and density of states, larger *k*-point meshes of 1 × 1 × 21 were adopted.

A ZCNS composed of *n* zigzag carbon atom chains was labeled by *n*-ZCNS (the corresponding ZGNR was labeled as *n*-ZGNR), and its initial atomic structure was constructed using the truncated Archimedean-type spiral form.[20,39] Initial inner radius of the CNS was represented by *r*, and the interlayer space *d* was set to 3.4 Å, which is close to the one of graphite. In order to simulate the rolling process of ZCNSs, its two edges need to be fixed, and were saturated by hydrogen atoms for avoiding the occurrence of dangling bonds. Two types of ZCNSs with the edges overlapped and non-overlapped, denoted as O-ZCNS and N-ZCNS, are shown in Fig. 1(a) and (b), respectively.

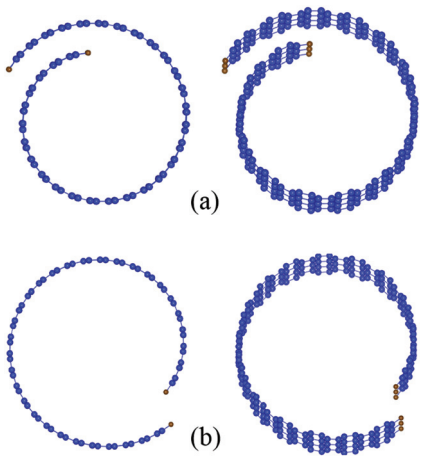

Fig. 1 Top (left panel) and perspective views (right panel) of initial structural models for (a) O-ZCNS and (b) N-ZCNS. The blue and brown balls represent C and H atoms, respectively.

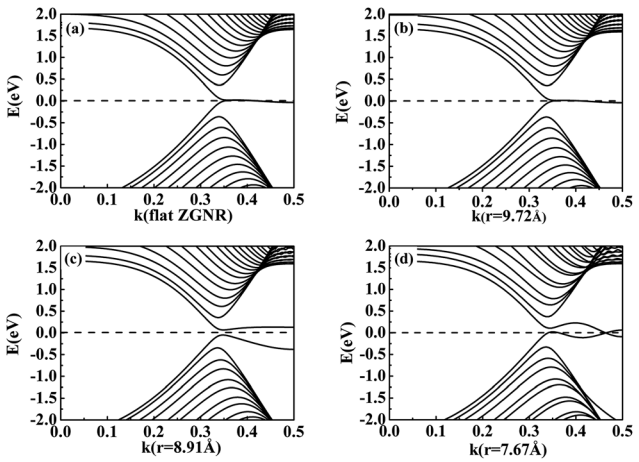

Fig. 2 Electronic band structures of (a) 32-ZGNR and three states of rolled ZGNRs with (b) r = 9.72 Å (N-ZCNS), (c) r = 8.91 Å (N-ZCNS) and (d) r = 7.67 Å (O-ZCNS). The Fermi level is denoted by a dashed line.

Results and discussion

As a typical example, 32-ZCNS is adopted to investigate the vibrations of electronic properties during its rolling process. After structural optimization, 32-ZCNS could be maintained with small distortions owing to the fixed edges. Fig. 2 shows the electronic band structures of the 32-ZGNR and three states of 32-ZCNSs. Obviously, the flat ZGNR (radius $r = +\infty$) exhibits metallic features with two bands crossing the Fermi level, which is well consistent with the previous work.[13] Similar metallic features are also preserved in N-ZCNS with the radius r = 9.72 Å [see Fig. 2(b)]. Of particular interest is that further decreasing r to 8.91 Å, the N-ZCNS exhibits a semiconductor with a small direct band gap, as shown in Fig. 2(c). As r equals 7.67 Å, two edges of the ZCNS are overlapped (*i.e.*, O-ZCNS). The highest valence band and lowest conduction band cross each other at the Fermi level, which results in the O-ZCNS exhibiting metallic features again, as depicted in Fig. 2(d). Probably, a metal–semiconductor–metal transition can be observed during the rolling process of 32-ZCNS.

For further clarifying the fantastic electronic properties, a series of rolled ZGNRs with different radii (*i.e.*, ZCNSs) are also

Table 1 Properties of flat (r = +∞) and rolled 32-ZGNRs: initial radius r (Å) and band gap E_g (meV) (N: non-overlapped edges, O: overlapped edges, E: electronic property, M: metal, and S: semiconductor)

r	+∞	9.72	9.45	9.18	9.10	9.02	8.91	8.64	8.53	8.10	7.83	7.67	7.56
Types	N	N	N	N	N	N	N	O	O	O	O	O	O
E_g	—	—	—	7.1	29.4	69.2	117	69.5	16	11.8	3.20	—	—
E	M	M	M	S	S	S	S	S	S	S	S	M	M

explored as listed in Table 1. It is found that for the case of r in the range of 9.18 to 7.83 Å, the ZCNSs are semiconductors and their band gaps increase first and then decrease with decreasing r, showing a maximum band gap of 117 meV at r = 8.91 Å. For other cases, that is, r greater than 9.18 Å or less than 7.83 Å, all the ZCNSs exhibit metallic properties. Therefore, the transition of metal–semiconductor–metal is the natural phenomenon of 32-ZCNS during its formation process.

As is well known, the band gaps of semiconductors are determined by the valence band maximum (VBM) and conduction band minimum (CBM). Analysis of partial charge density and density of states (DOS) at both the VBM and CBM are helpful to explore the origin of the metal–semiconductor–metal transition. Fig. 3 displays the spatial charge distributions of the Fermi level for metallic ZCNSs and those of the VBM and CBM for semiconducting ZCNSs. For the metallic systems with r = 9.72 and 7.56 Å shown in Fig. 3(a) and (d), the spatial charge distributions are mainly contributed by the two edges. For both the semiconductors of N-ZCNS (r = 9.02 Å) and O-ZCNS (r = 8.53 Å), their VBMs and CBMs are also dominated by the two edges with few parts from the regions near the edges, as presented in Fig. 3(b) and (c). In other ZCNSs, analogous charge contributions are also observed at the Fermi level or the VBMs and CBMs. Thereby, it can be clearly inferred that interaction between the two edges of 32-ZCNS plays a key role in the metal–semiconductor–metal transition.

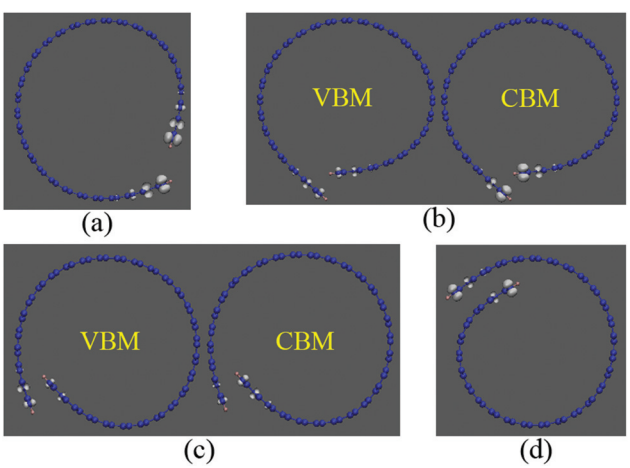

Fig. 3 Partial charge density at the Fermi level of metallic ZCNSs with (a) r = 9.72 Å and (d) r = 7.56 Å, and at the VBM and CBM of semiconducting ZCNSs with (b) r = 9.02 Å and (c) r = 8.53 Å.

As representative examples, partial DOSs of metallic N-ZCNS with r = 9.72 Å and semiconducting N-ZCNS with r = 9.02 Å are shown in Fig. 4(a) and (b), respectively. It can be seen from Fig. 4(a) that the Fermi level of the metallic N-ZCNS is mainly contributed by the C p orbital of the edges in spite of the two edges saturated by H atoms. For the semiconducting N-ZCNS shown in Fig. 4(b), both the VBM and CBM are also dominated mostly by the edge C p orbital. In other words, the electronic contributions of O-ZCNSs are similar to those of N-ZCNSs whether they are metallic or semiconducting (see Fig. S1†). Owing to the interaction of the C p orbital between the two edges, a small band gap of 7.10 meV opens when the radius r of the ZCNS reaches 9.18 Å (see Table 1). Furthermore, as r decreases from 9.18 to 8.91 Å, the interaction between the two edges become stronger, which can be deduced from the inversely proportional relationship between total energy and d_{C-C} (*i.e.*, distance between two edges), as shown in Fig. 4(c). This results in band gaps up to several tens of meV. Taking the N-ZCNS with r = 8.91 Å as an example, its band gap is 117 meV. Subsequently, as r decreases to 7.83 Å, the band gaps decrease to 3.20 meV because of the weaker interaction between the two edges. When r is smaller than 7.83 Å, the

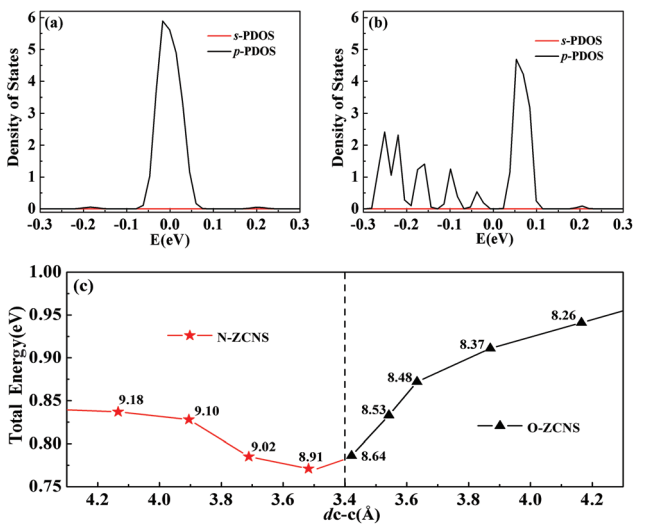

Fig. 4 Partial density of states (PDOSs) of the edge C atoms for (a) metallic N-ZCNS with r = 9.72 Å and (b) semiconducting N-ZCNS with r = 9.02 Å. The Fermi level is set to zero. (c) Partial relationship of total energy with d_{C-C} (the distance between two edges). The energy is relative to that of ZGNR. Numerical values in (c) present the corresponding initial radii r (unit in Å).

ZCNS exhibits metallic features again. Therefore, we can conclude that the interaction of the C p orbital between the two edges induces 32-ZCNS showing a metal–semiconductor–metal transition.

Considering that the interaction between the two edges of ZCNS might be the long-range one, the van der Waals density functional (vdW-DF) approach has been employed to examine our results.[40] The generalized gradient approximation (GGA) with the functional of Perdew–Burke–Ernzerhof (PBE) is used to describe the exchange–correlation interaction.[41] It is found that the metal–semiconductor–metal transition can still occur during the rolling process of 32-ZGNR, regardless of the van der Waals interaction.

Next, the band gaps of 32-ZCNSs as a function of d_{C-C} are investigated and shown in Fig. 5. It should be pointed out that during the process of rolling ZGNRs into ZCNSs, d_{C-C} decreases first and then increases when the two edges are overlapped. Combining with the energy variations in Fig. 4(c), one can see that the 32-ZGNR without any bending deformation has the largest d_{C-C}, displaying the weakest interaction between the two edges, and exhibits metallic properties. Once a bending strain is applied to 32-ZGNR, it could evolve into a ZCNS with a smaller d_{C-C}. Generally, the increase of curvature in a CNS results in the bending energy rising, which would enhance the total energy.[5,10,19,32,42] Whereas, for r reducing from 9.45 to 8.91 Å, the total energy of the ZCNS decreases. This can be illustrated that with the increasing curvature, d_{C-C} decreases and the interaction between the two edges strengthens, leading to the total energy descending. As d_{C-C} drops to 4.134 Å, the strengthened interaction results in the ZCNS possessing semiconductor characteristics. When d_{C-C} reaches the smallest value (3.421 Å), the interaction is the strongest. However, the band gap of the ZCNS is not the largest, which is probably induced by the curvature effects. Afterwards, owing to the gradual strengthened curvature effects and weakened interaction between the two edges, the band gap decreases slowly and disappears finally, and then metallic features occur again in the ZCNS. It is known that as the radius of the ZCNS becomes smaller, curvature effects will be stronger. Although the interaction between the two edges dominates the electronic properties of the ZCNSs, different curvatures in N-ZCNSs and O-ZCNSs will result in an asymmetrical trend of band gap according to d_{C-C} = 3.4 Å, as illustrated in Fig. 5.

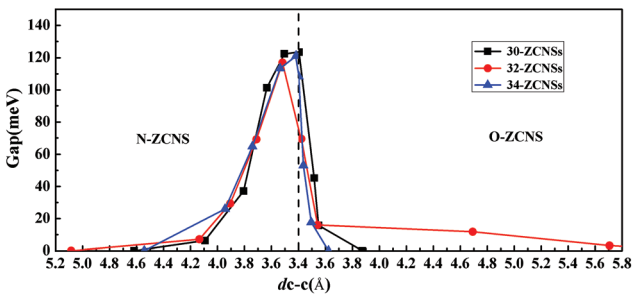

Fig. 5 Relationships of band gaps with d_{C-C} in ZCNSs. Left and right sides of the dashed line represent N-ZCNSs and O-ZCNSs.

In order to examine the dependence of metal–semiconductor–metal transition on the ribbon width, electronic properties of the other two systems, that is, 30-ZGNR and 34-ZGNR, during their rolling processes have been explored. Their band gaps against d_{C-C} are shown in Fig. 5. Similar to the rolled 32-ZGNR, the maximum band gaps of 123 and 121 meV are presented for the rolled 30-ZGNR and 34-ZGNR with d_{C-C} = 3.404 and 3.417 Å, respectively. When d_{C-C} exceeds 4.09 Å, the band gaps disappear and all ZCNSs with their edges overlapped or non-overlapped are metallic. Thereby, the transition of metal–semiconductor–metal still arises in both rolled 30-ZGNR and 34-ZGNR and can be explained in the same formalism of rolled 32-ZGNR.

Of particular interest and importance is that previous studies have demonstrated that in graphene, spin–orbit interaction (SOI) can be strengthened by bending deformation and induces a band gap opening.[43–45] Thus, one may ask what about the effects of SOI on the electronic properties of the rolled ZGNRs? To explore this issue, traditional DFT calculations within SOI are employed, and the band gaps are listed in Table 2. Compared with the band structures shown in Fig. 2, those based on SOI exhibit little difference with some bands splitting, which results in the band gaps disappearing at d_{C-C} = 4.692, 3.905, and 4.134 Å, while enlarging at d_{C-C} = 3.54 and 3.711 Å. A metal–semiconductor–metal transition can still be observed in the formation process of ZCNSs rolled from ZGNRs.

Our results of the metal–semiconductor–metal transition in ZCNSs are robust, and independent of the ribbon width and SOI. Such a metal–semiconductor–metal transition suggests an opportunity of band engineering in ZCNSs and may open their potential applications in nano-electromechanical devices. In addition, according to our results, it is reasonable to explain why multilayered ZCNSs exhibit metallic features in previous studies.[22] Because the Fermi levels of these ZCNSs are mainly dominated by their two edges, and the distance between the two edges is too large to form strong interactions, the multilayered ZCNSs exhibit metallic features.

Table 2 Properties of 32-ZCNSs with the spin–orbit interactions (N: non-overlapped edges, O: overlapped edges). d_{C-C} (Å) represents the distance between two edges. E_g and $E_{g\text{-}SOI}$ (meV) are the band gaps without and with the spin–orbit interaction

d_{C-C}	6.216	4.134	3.905	3.711	3.518	3.54	4.692	6.8
Types	N	N	N	N	N	O	O	O
E_g	—	7.1	29.4	69.2	117	16	11.8	—
$E_{g\text{-}SOI}$	—	—	—	113	116.3	33.6	—	—

Conclusions

In summary, first-principles calculations have been employed to systematically investigate the effects of bending deformation on the electronic properties of ZCNSs during the rolling process from ZGNRs. We have found that a metal–semiconductor–metal transition can occur in the ZCNSs under the bending deformation. By analyzing the partial charge density and the density of states, such an electronic property transition mainly depended on the interaction of the C p orbital between the two edges of ZCNSs. Furthermore, the metal–semiconductor–metal transition in the ZCNSs is valid and independent of the ribbon width as well as SOI. Based on our results, we can also explain reasonably why a multilayered ZCNS is a metal.

Acknowledgements

The authors thank M. G. Xia, K. Zhang, H. W. Chen and X. Chen for helpful discussions. This work is supported by the Cultivation Fund of the Key Scientific and Technical Innovation Project Ministry of Education of China (Grant No. 708082) and the National Natural Science Foundation of China (NSFC) (Grant No. 11074196, 11374237, 11204232, and 11304241).

Notes and references

1 R. Bacon, *J. Appl. Phys.*, 1960, **31**, 283–290.
2 Z. F. Wang, Q. W. Shi, Q. Li, X. Wang, J. G. Hou, H. Zheng, Y. Yao and J. Chen, *Appl. Phys. Lett.*, 2007, **91**, 053109.
3 G. Shan, X. Zhao and W. Huang, *J. Nanoelectron. Optoelectron.*, 2011, **6**, 138–143.
4 Y. Huang and T. Li, *J. Appl. Mech.*, 2013, **80**, 040903.
5 X. Shi, Q. Yin, N. M. Pugno and H. Gao, *J. Appl. Mech.*, 2014, **81**, 021014.
6 V. R. Coluci, S. F. Braga, R. H. Baughman and D. S. Galvao, *Phys. Rev. B: Condens. Matter*, 2007, **75**, 125404.
7 S. F. Braga, V. R. Coluci, R. H. Baughman and D. S. Galvao, *Chem. Phys. Lett.*, 2007, **441**, 78–82.
8 X. Shi, Y. Cheng, N. M. Pugno and H. Gao, *Appl. Phys. Lett.*, 2010, **96**, 053115.
9 Z. Zhang and T. Li, *Nanoscale. Res. Lett.*, 2011, **6**, 470.
10 X. Shi, N. M. Pugno, Y. Cheng and H. Gao, *Appl. Phys. Lett.*, 2009, **95**, 163113.
11 F. Zeng, Y. Kuang, G. Liu, R. Liu, Z. Huang, C. Fu and H. Zhou, *Nanoscale*, 2012, **4**, 3997–4001.
12 K. Nakada, M. Fujita, G. Dressslhaus and M. S. Dresselhaus, *Phys. Rev. B: Condens. Matter*, 1996, **54**, 17954–17961.
13 M. Fujita, K. Wakabayashi, K. Nakada and K. Kusakabe, *J. Phys. Soc. Jpn.*, 1996, **65**, 1920–1923.
14 L. Yang, C.-H. Park, Y.-W. Son, M. L. Cohen and S. G. Louie, *Phys. Rev. Lett.*, 2007, **99**, 186801.
15 D. A. Abanin, P. A. Lee and L. S. Levitov, *Phys. Rev. Lett.*, 2006, **96**, 176803.
16 X. Lu and Z. Chen, *Chem. Rev.*, 2005, **105**, 3643–3696.
17 D. Xia, Q. Xue, J. Xie, H. Chen, C. Lv, F. Besenbacher and M. Dong, *Small*, 2010, **6**, 2010–2019.
18 K. Yan, Q. Xue, D. Xia, H. Chen, J. Xie and M. Dong, *ACS Nano*, 2009, **3**, 2235–2240.
19 X. Shi, N. M. Pugno and H. Gao, *J. Comput. Theor. Nanosci.*, 2010, **7**, 1–5.
20 L. Lai, J. Lu, L. Wang, G. Luo, J. Zhou, R. Qin, Y. Chen, H. Li, Z. Gao, G. Li, W. N. Mei, Y. Maeda, T. Akasaka and S. Sanvito, *Nano Res.*, 2009, **2**, 844–850.
21 Y. Chen, J. Lu and Z. Gao, *J. Phys. Chem. C*, 2007, **111**, 1625–1630.
22 H. Pan, Y. Feng and J. Lin, *Phys. Rev. B: Condens. Matter*, 2005, **72**, 085415.
23 X. Xie, L. Ju, X. Feng, Y. Sun, R. Zhou, K. Liu, S. Fan, Q. Li and K. Jiang, *Nano Lett.*, 2009, **9**, 2565–2570.
24 A. K. Schaper, H. Hou, M. Wang, Y. Bando and D. Golberg, *Carbon*, 2011, **49**, 1821–1828.
25 E. Perim, R. Paupitz and D. S. Galvao, *J. Appl. Phys.*, 2013, **113**, 054306.
26 Y. Wang, H. F. Zhan, C. Yang, Y. Xiang and Y. Y. Zhang, *Comput. Mater. Sci.*, 2015, **96**, 300–305.
27 J. G. Lavin, S. Subramoney, R. S. Ruoff, S. Berber and D. Tomanek, *Carbon*, 2002, **40**, 1123–1130.
28 D. Tománek, W. Zhong and E. Krastev, *Phys. Rev. B: Condens. Matter*, 1993, **48**, 15461–15464.
29 D. Tománek, *Phys. B*, 2002, **323**, 86–89.
30 M. Grundmann, *Appl. Phys. Lett.*, 2003, **83**, 2444–2446.
31 Z. Xu and M. J. Buehler, *ACS Nano*, 2010, **4**, 3869–3876.
32 S. F. Braga, V. R. Coluci, S. B. Legoas, R. Giro, D. S. Galvao and R. H. Baughman, *Nano Lett.*, 2004, **4**, 881–884.
33 H. Y. Song, S. F. Geng, M. R. An and X. W. Zha, *J. Appl. Phys.*, 2013, **113**, 164305.
34 G. Kresse and J. Furthmüller, *Comput. Mater. Sci.*, 1996, **6**, 15–50.
35 G. Kresse and J. Furthmüller, *Phys. Rev. B: Condens. Matter*, 1996, **54**, 11169–11186.
36 P. E. Blöchl, *Phys. Rev. B: Condens. Matter*, 1994, **50**, 17953–17979.
37 W. Kohn and L. Sham, *Phys. Rev.*, 1965, **140**, A1133–A1138.
38 H. J. Monkhorst and J. D. Pack, *Phys. Rev. B: Condens. Matter*, 1976, **13**, 5188–5192.
39 T. S. Li, M. F. Lin and J. Y. Wu, *Philos. Mag.*, 2011, **91**, 1557–1567.
40 M. Dion, H. Rydberg, E. Schroder, D. C. Langreth and B. I. Lundqvist, *Phys. Rev. Lett.*, 2004, **92**, 246401.
41 J. P. Perdew, K. Burke and M. Ernzerhof, *Phys. Rev. Lett.*, 1997, **78**, 1396.
42 Q. Yin and X. Shi, *Nanoscale*, 2013, **5**, 5450–5455.
43 O. Seiichiro, I. Yasuhito, K. Hiroshi and J.-I. Inoue, *Phys. Rev. B: Condens. Matter*, 2008, **78**, 121403.
44 M. Gmitra, S. Konschuh, C. Ertler, C. Ambrosch-Draxl and J. Fabian, *Phys. Rev. B: Condens. Matter*, 2009, **80**, 235431.
45 D. Huertas-Hernando, F. Guinea and A. Brataas, *Phys. Rev. B: Condens. Matter*, 2006, **74**, 155426.